Seismicity distribution and locking depth along the Main Marmara Fault, Turkey

Jean Schmittbuhl, H. Karabulut, O. Lengline, M. Bouchon

AGU PUBLICATIONS

Geochemistry, Geophysics, Geosystems

RESEARCH ARTICLE
10.1002/2015GC006120

Seismicity distribution and locking depth along the Main Marmara Fault, Turkey

J. Schmittbuhl[1], H. Karabulut[1,2], O. Lengliné[1], and M. Bouchon[3]

[1]EOST, CNRS/Université de Strasbourg, Strasbourg, France, [2]KOERI, Bogazici University, Istanbul, Turkey, [3]ISTerre, CNRS/Université Joseph Fourier, Grenoble, France

Key Points:
- Long-term seismicity monitoring of the Main Marmara Fault
- Evidences of deep creeping in the Central basin
- Implications for the seismic hazard of Istanbul

Correspondence to:
J. Schmittbuhl,
Jean.Schmittbuhl@unistra.fr

Citation:
Schmittbuhl, J., H. Karabulut, O. Lengliné, and M. Bouchon (2015), Seismicity distribution and locking depth along the Main Marmara Fault, Turkey, *Geochem. Geophys. Geosyst.*, *17*, 954–965, doi:10.1002/2015GC006120.

Received 6 OCT 2015
Accepted 2 DEC 2015
Accepted article online 9 DEC 2015
Published online 18 MAR 2016

Abstract The seismicity along the Main Marmara Fault (MMF) below the Marmara Sea is analyzed during the 2007–2012 period to provide insights on the recent evolution of this important regional seismic gap. High precision locations show that seismicity is strongly varying along strike and depth providing fine details of the fault behavior that are inaccessible from geodetic observations. The activity strongly clusters at the regions of transition between basins. The Central basin shows significant seismicity located below the shallow locking depth inferred from GPS measurements. Its *b*-value is low and the average seismic slip is high. All observations are consistent with a deep creep of this segment. On the contrary, the Kumburgaz basin at the center of the fault shows sparse seismicity with the hallmarks of a locked segment. In the eastern Marmara Sea, the seismicity distribution along the Princes Island segment in the Cinarcik basin, is consistent with the geodetic locking depth of 10 km and a low contribution to the regional seismic energy release. The assessment of the locked segment areas provide an estimate of the magnitude of the main forthcoming event to be about 7.3 assuming that the rupture will not enter significantly within creeping domains.

1. Introduction

The North Anatolian Fault (NAF) poses a significant hazard for the large cities surrounding the Marmara Sea region particularly the megalopolis of Istanbul. Indeed, the NAF is presently hosting a long unruptured segment below the Sea of Marmara. This seismic gap is approximately 150 km long and corresponds to the Main Marmara Fault (MMF). Since the 1999 Izmit earthquake which ruptured the eastern segment to the gap, scientists have been involved in the monitoring of the activity of the fault, using a large spectrum of techniques [*McClusky et al*., 2000; *Imren et al*., 2001; *Geli et al*., 2008; *Çakir et al*., 2012]. One of the principal issues for seismic hazard assessment in the region is to know if the MMF is totally or partly locked [*Bohnhoff et al*., 2013; *Ergintav et al*., 2014]. Along locked segments, faults accumulate strain energy which is relaxed abruptly during major earthquakes. Alternatively as suggested by several recent studies [*Karabacak et al*., 2011; *Çakir et al*., 2012], there are also fault segments along the NAF that relax part of their tectonic loading continuously in a creeping mode without significant seismic activity. In this second mode, the accumulated strain energy is expected to be significantly reduced. Recently, *Ergintav et al*. [2014] suggested that such a creeping segment exists in the central part of the MMF.

A first-order quantification of the partition between deformation modes along the fault (i.e., creeping or locked) is the coupling coefficient. It measures the percentage of deformation accommodated by seismic events. In the Marmara Sea region, the coupling coefficient is actually difficult to assess because of the insufficient knowledge of geodetic and seismic strain releases over the last seismic cycle (∼250 year). An alternative for stick-slip fault, as classically introduced in geodesy, is to calculate from GPS profiles, the locking depth that separates the upper part of the fault which is supposed to be homogeneously locked and elastically loaded, and the lower part which is fully creeping [e.g., *Segall*, 2010]. Typically the locking depth is rather shallow in the Marmara region, 6–7 km [*Meade et al*., 2002; *Ergintav et al*., 2007]. But a major challenge is the presence of the Marmara Sea that conceals the MMF trace and significantly limits the measurements of the fault strain. On the contrary to well-instrumented zones like the San Andreas Fault [*Savage and Burford*, 1973; *Fialko*, 2006], triangulation networks or creep-meters or high resolution InSAR images cannot

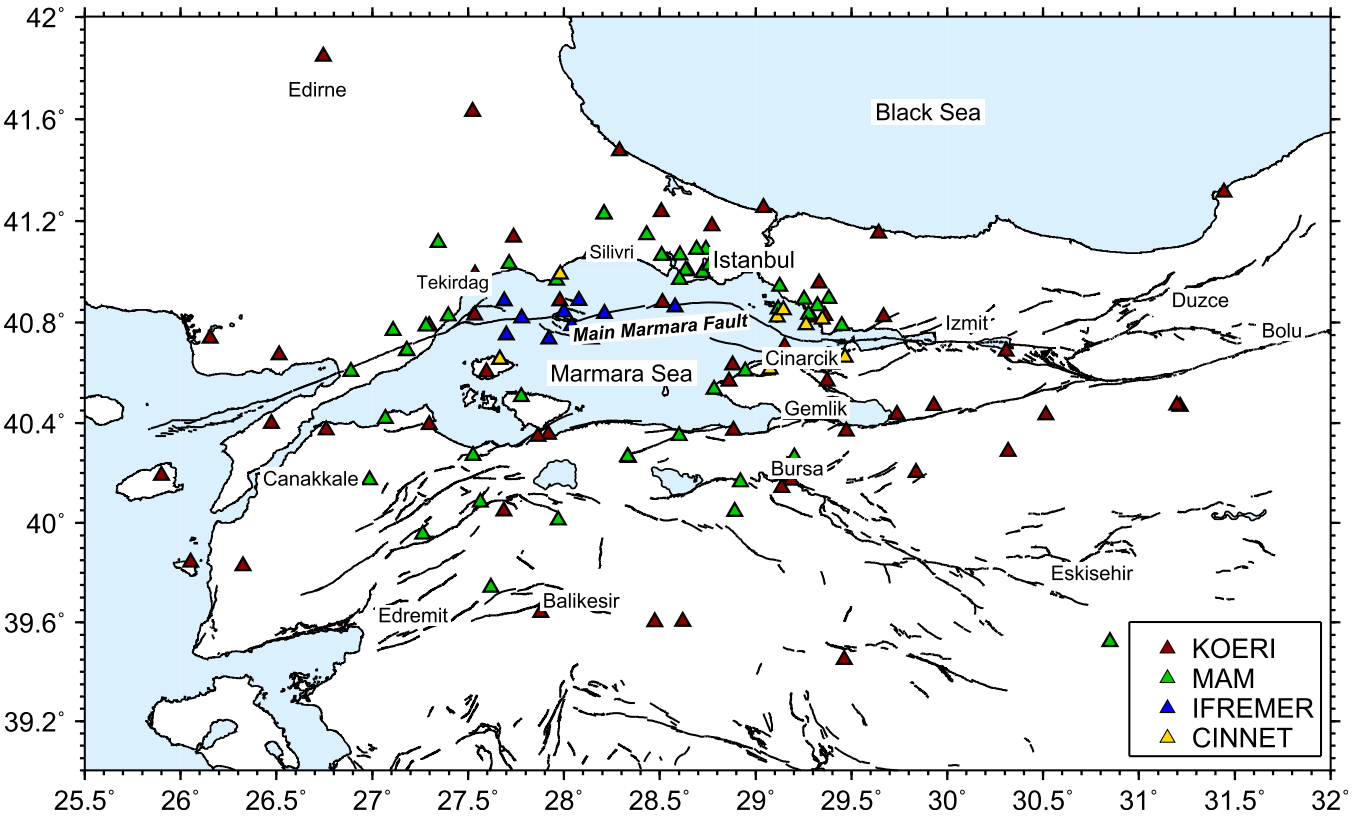

Figure 1. Map of 124 (out of the 132) seismic stations around the Marmara Sea used for this study from two permanent networks (KOERI and MAM) and two temporary networks (IFREMER and CINNET). The eight stations used and not shown are on the south of this zone. Fault network is from *Emre et al.* [2013].

be made along this major strike-slip fault trace. An important concern is to know what can still be assessed with limited geodetic data.

While geodetic records give long term and large-scale information, microseismicity might be seen as a natural tracer of the on-going fault deformation on a much finer scale. It provides complementary information related to local in situ processes [*Waldhauser et al.*, 2004; *Lengliné and Marsan*, 2009; *Lengliné et al.*, 2012]. Numerous works on large strike faults such as the San Andreas Fault have shown from seismicity data the duality of the fault behavior (creeping or locked). Moreover, it is shown to exist not only through depth but also with strong lateral variations [*Wdowinski*, 2009; *Shelly*, 2010]. It is worth pointing out that fault behavior can also depend on the time in the earthquake cycle (e.g., for the Izmit fault) [*Çakir et al.*, 2012]. However, the interpretation of microseismicity distribution in terms of fault mechanics is often limited by the low precision of earthquake locations [e.g., *Rubin et al.*, 1999]. It requires in particular a good network coverage and important detection capabilities.

The objective of the present study is to provide a high resolution analysis of the seismicity distribution along the MMF during the 2007–2012 period and to link it to geodetic observations. We first identify domains along the fault with coherent behaviors. We show the extent of the seismogenic zone both in time and space and compare it to the geodetic locking depth. We study the lateral variations of statistical properties of microseismicity (i.e., background seismic rate, *b*-values, seismic slip distribution). We identify swarms that might host the nucleation of the next major event [*Bouchon et al.*, 2011] or mark the barriers to large earthquake ruptures [*Reverso et al.*, 2015]. Finally, we discuss the present seismotectonic behavior of the MMF.

2. Methods

We used seismic waveform data that were acquired between 2007 and 2012. The data were compiled from 132 seismic stations belonging to local permanent and temporary networks. The map of the seismic

stations used for this study is shown in Figure 1. It includes broadband stations operated by Kandilli Observatory and Earthquake Research Institute (KOERI) and MAM-TUBITAK (the Scientific and Technological Research Council of Turkey), the short period CINNET stations supported by ANR (the French National Research Agency), stations installed during the REAKT project by KOERI, the permanent cabled KOERI OBS stations, and the temporary OBS stations from IFREMER (French Research Institute for Exploitation of the Sea).

The starting date of 2007 was chosen because of the increase of the station density around the Cinarcik basin at that period. Detection windows have been obtained from an STA/LTA procedure [*Earle and Shearer*, 1994]. We manually picked *P* and *S* wave arrivals on all detection windows for which we could identify a clear phase arrival. The earthquake location has been performed from the SEISAN, HYPOCENTER program [*Lienert and Havskov*, 1995; *Havskov and Ottemoller*, 1999] assuming a 1-D velocity model [*Karabulut et al*., 2011]. In order to improve the absolute location of the earthquakes, stations delays are also estimated from the VELEST software [*Kissling et al*., 1994] and introduced in the location.

The location procedure has been performed independently for two separate regions of the MMF. The first region comprises the eastern part of the Marmara Sea. It includes the Cinarcik basin and extends westward to the Istanbul area. In this region, we located 3092 events with a mean RMS error of 0.09 s. The second area comprises the western Marmara Sea and overlaps with the other region at the longitude of the city of Istanbul. In this area, we located 1489 events with a mean RMS error of 0.12 s. Numerous events from quarry blasts have been removed as being shallow daily clusters of events. The obtained earthquake catalog for the whole Marmara region consists of 4581 events in the region defined in Figure 1. It includes 1936 events along the MMF zone defined as a roughly 10 km thick region around the fault trace proposed by *Le Pichon et al*. [2001] (the zone is broader to the west in the Tekirdag domain where secondary subparallel faults to the MMF exist). Typical absolute errors in longitude, latitude, and depth are 1 km, 1 km and 3 km, respectively.

For both regions, earthquakes are then relocated using the HYPODD software [*Waldhauser and Ellsworth*, 2000]. We first computed time delays for all possible pairs of earthquakes. This is achieved by computing the time correlation function on 256 samples long signals of two earthquakes at a common station on the vertical component. All windows start 100 samples before the *P* wave pick and all signals are first filtered in the [3–20] Hz frequency band. We retain all estimated delays when the maximum of the correlation function reaches a value of 0.8 or higher. Cross-correlation *P* wave travel time delays were associated with *P* and *S* waves delays computed from the picked arrival times. We finally relocated 3830 events out of the initial 4581 locations. Local magnitudes (M_l) were estimated by first removing the instrument response and then extracting the maximum amplitude of the signal convolved with a Wood Anderson response. Figure 2a shows the geographical and depth distribution of the seismicity.

We compared our catalog to the KOERI catalog obtained from permanent stations only (see Appendix A) (http://www.koeri.boun.edu.tr/sismo). We observed that our catalog contains in the MMF region twice as many events (colored circles in Figures 2 and A1). Both figures share similarities like a very sparse distribution in the Kumburgaz domain but map and depth sections from our catalog show clearly more focused event distribution and a larger range of magnitudes. Figure A2 compares the distributions of event magnitudes for the MMF region using: (1) all events of the present catalog in the defined region, (2) events of the present catalog that also exist in the KOERI catalog, and (3) events of the KOERI catalog. All distributions were fitted using the same maximum-likelihood method described by *Ogata and Katsura* [1993] assuming the observed frequency distributions to be constant in time and space within the prescribed domain. Using the same procedure provides estimates of M_c and *b*-values that can be quantitatively compared. First, we were able to significantly reduce the completeness magnitude of our catalog from $M_c \sim 3.2$ to $M_c \sim 1.9$ over the whole MMF and to obtain a relevant *b*-value: $b = 0.94 \pm 0.07$. Interestingly, using events from our catalog with similar origin times and locations as the KOERI catalog provides an intermediate $M_c = 2.4$ and a comparable *b*-value: $b = 1.06 \pm 0.12$. We inferred from this comparison that the KOERI catalog has an inaccurate magnitude estimation particularly for small events which might be related to the limited azimuth coverage of the KOERI network. Applying our magnitude computation on the KOERI events provides a significant improvement of the event distribution and magnitude completeness. Accordingly the catalog proposed here allows for monitoring at best the fine details of the recent seismic activity along the MMF.

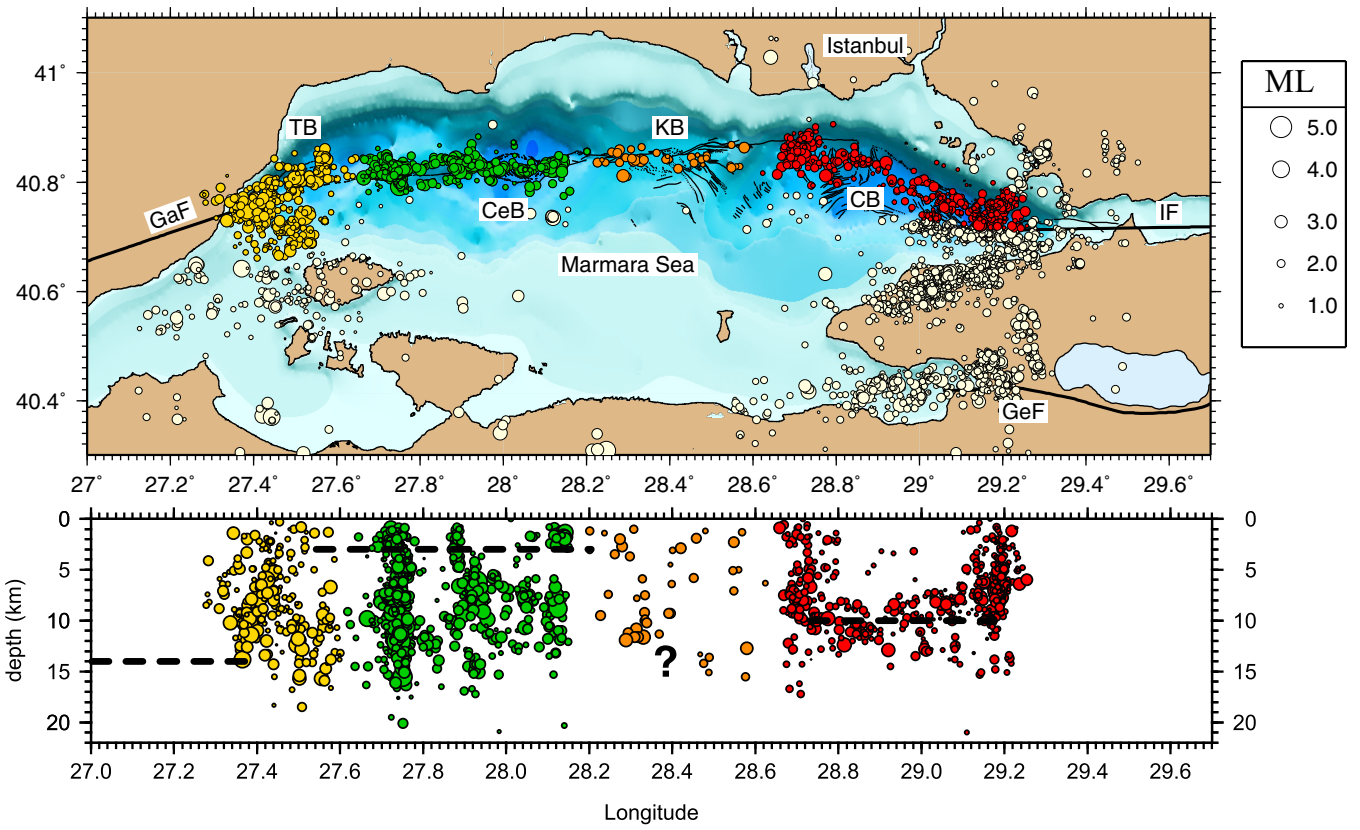

Figure 2. (top) Map and (bottom) cross section of the seismicity along the Main Marmara Fault during the period 2007–2012. Four domains are introduced: the Tekirdag basin (TB) in yellow, the Central basin (CeB) in green, the Kumburgaz basin (KB) in orange, and the Cinarcik basin (CB) in red. All the regional seismicity away from the MMF is plotted in white. Bathymetry is from *Armijo et al*. [2005]. Fault network is from *Le Pichon et al*. [2001] (GaF for Ganos fault, IF for Izmit fault, and GeF for Gemlik fault). Geographical details are in Figure 1. Dotted lines in the depth section show the geodetically estimated locking depth of each domain (see text for references).

3. Results

3.1. Four Segments Along the MMF

Based on the geographical and depth distribution of microseismicity between 2007 and 2012, four segments are defined along the MMF (see Figure 2) corresponding to the four major basins of the Marmara Sea. To the west, in the Tekirdag basin (TB) and Central basin (CeB), seismicity is abundant and distributed over a wide depth range (from surface to 17 km). At the transition between TB and CeB (see Figure 2 at longitude 27.74° corresponding to the Western High) [*Le Pichon et al*., 2001] we observe numerous earthquakes along a very extended cluster in depth. They are possibly related to fault offsets. As noted by *Weaver and Hill* [1978] for the San Andreas Fault system, the depth extension h of a seismic cluster can be related to the fault offset l: $h/l \approx 1$. Following this argument, it suggests that a significant complexity of the MMF trace exists there.

To the east, in the Cinarcik basin (CB), seismicity is geographically uniformly distributed along the Princes Islands (PI) segment. It spreads within a narrow depth range between 8 and 14 km except at both ends of this basin where the seismicity extends vertically up to the surface as recently observed by *Bohnhoff et al*. [2013]. To the west, the extended seismic cluster corresponds to the kink of the MMF where its strike exhibits a significant change from a NW-SE to a E-W. In the eastern Marmara, the seismic cluster is located in the Tuzla region at the transition with the Izmit fault corresponding to a local complex structure. For both clusters of this segment (i.e., the kink cluster and the Tuzla cluster), the argument of *Weaver and Hill* [1978] about the link between fault offset and depth extension of seismic clusters is then expected to hold.

On the contrary, in the Kumburgaz basin (KB) located in the center of the Marmara Sea, seismicity is very sparse. It is of interest to see that it shares similarities with the ruptured Ganos segment

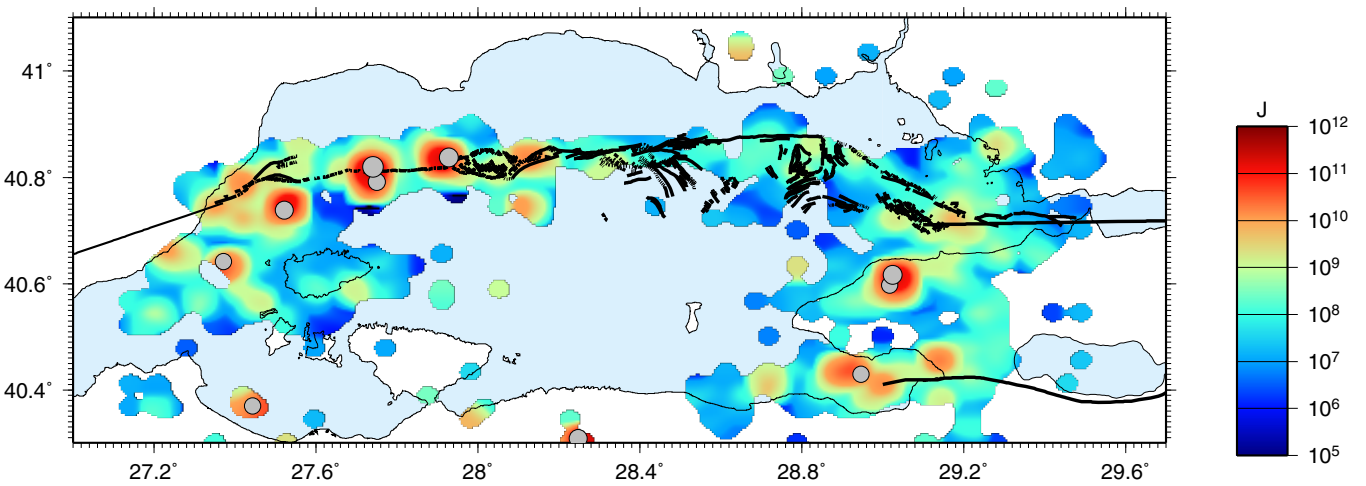

Figure 3. Cumulative seismic energy map using the relationship from *Kanamori and Anderson* [1975] between seismic energy and magnitude: $E=10^{1.5M+4.8}$. Energy is accumulated from 1 January 2007 to 31 December 2012. The largest events ($M \geq 4$) are superimposed in gray. Fault network is from *Le Pichon et al.* [2001].

(1912 earthquake) to the west and the Izmit segment (1999 earthquake) to the east where there is also very little seismicity.

3.2. Seismic Energy Map

In order to estimate the relative importance of the seismicity in the different subregions of the Marmara Sea, we computed the cumulative seismic energy from 2007 to 2012 using the relationship from *Kanamori and Anderson* [1975]: $E=10^{1.5M+4.8}$ between the seismic energy E and the magnitude M (see Figure 3). The geographical grid for this computation is $[0.035^\circ, 0.022^\circ]$, respectively, in longitude and latitude. There is no estimate where no event was detected. Also the largest seismic events $M \geq 4$ are superimposed in gray in the figure. First, we see from Figure 3, that zones of high seismic energy release are typically related to the presence of a large event as expected, but they are not all related to the MMF. The Yalova-Cinarcik activity on the south of the Cinarcik basin is a good example. The western termination of the Gemlik fault is another. Second, only the western part of the MMF, in the Tekirdag (TB) and the Central basin (CeB), is hosting major regional events. It makes a significant difference with the eastern part of the MMF, i.e., the Princes Islands (PI) where the abundant seismicity is not really contributing to the regional seismic energy release. Interestingly, zones of high energy release on the west side of the MMF (in the TB and CeB) are regularly spaced by a typical distance of the order of 20 km which is significantly larger than the rupture length of the largest event in the clusters.

The lack of moderate earthquakes in the eastern Marmara Sea is consistent with a spatially diffuse activity in the Cinarcik basin over at least four main structures from north to south: the PI segment of the MMF, the termination of the Izmit Fault in the Cinarcik basin, the Yalova-Cinarcik cluster, and the Gemlik fault (as clearly shown in Figure 2 when summing the red and white dots on the right part of the figure between longitudes 28.8° and 29.3°). In this region, most of the events have normal fault mechanisms as shown in *Bulut et al.* [2009] and *Karabulut et al.* [2011]. It reflects that only part of the regional tectonic loading is released by the MMF segment in the Cinarcik basin as proposed from GPS inversion by *Hergert and Heidbach* [2010]. On the contrary, the deformation in the western Marmara region is localized mostly along the MMF except at the very western termination of the fault where a diffuse activity exists around the Marmara Island possibly related to the South Marmara Fault [*Le Pichon et al.*, 2014].

3.3. Depth Distribution and Locking Depth

In order to characterize the seismogenic zone of the MMF, we compute the depth distribution of the seismicity for the four segments and its evolution with time (see Figure 4). Depth extent is stationary in time and shows a clear cut-off at a depth that defines the seismogenic depth d_s. We estimated d_s from the 90% cumulative depth distribution: for TB, CeB, and KB, $d_s \sim 13$ km and for CB: $d_s \sim 11$ km (Figure 4). We note that in the Kumburgaz basin, the sparse seismicity is rather evenly distributed in time and depth which confirms that the location accuracy is homogeneous in time and space, with no loss of sensitivity with depth or

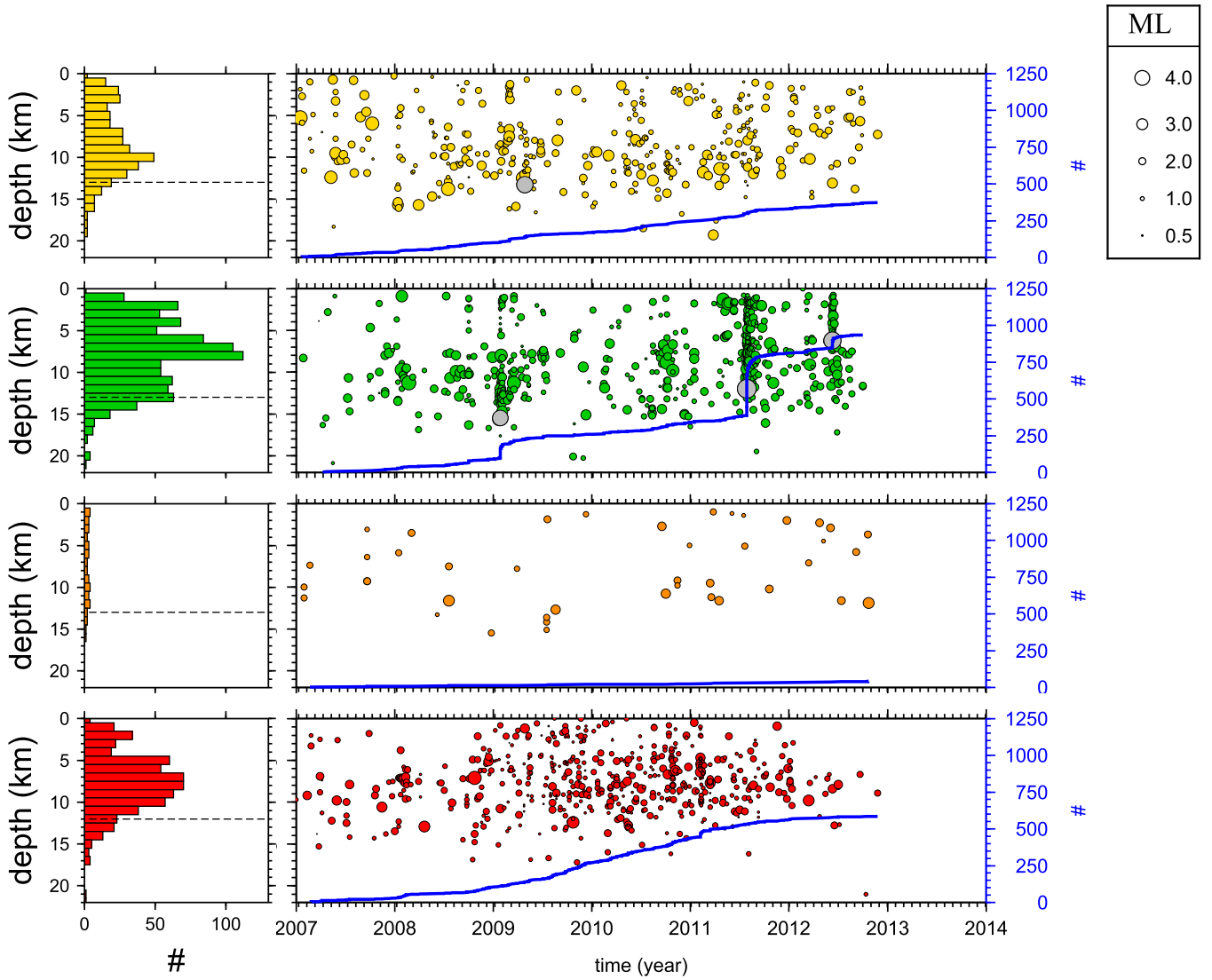

Figure 4. (left) Depth and (right) depth-time distribution of the MMF seismicity along the four domains of the Marmara Sea (same colors as in Figure 2). From top to bottom: Tekirdag basin (TB), Central basin (CeB), Kumburgaz basin (KB), and Cinarcik basin (CB). On the depth distributions, the horizontal dotted line corresponds to the seismogenic depth defined as the 90% limit of the cumulative distribution. Largest events ($M \geq 4$, shown in Figure 3) are superimposed in gray. Superimposed in blue is the cumulative number of events since 1 January 2007.

during specific time periods. We also checked that the magnitude of completeness does not change with depth such that the lower limit of seismicity reflects a real transition and not a low detection capability. In both western and eastern domains, the seismicity is maximum at around 8 km depth and decreases significantly at shallower depths. However gas or fluid induced seismicity in the sediments are possible and might explain the shallow activity [*Geli et al*., 2008].

Geodetic measurements along strike-slip faults are typically interpreted by assuming two domains in the crust: the upper and the lower crust, separated in simple models by a no-thickness brittle-ductile transition at the so-called locking depth [e.g., *Segall*, 2010]. Seismicity is assumed to develop above this locking depth, where the brittle and velocity weakening mechanisms prevail. Below the locking depth, the crust is expected to respond to the plate driving force ductily following velocity strengthening processes with no seismicity. A precise locking depth is difficult to assess geodetically in the Marmara Sea region owing to the lack of GPS stations close to the fault. When estimated at large scale (i.e., the Marmara Sea scale), the locking depth is relatively small (6–7 km) considering a southern path of the MMF and even smaller (2–3 km) when the fault trace includes the details of the present study [*Meade et al*., 2002]. However, at smaller scale, i.e., the basin scale, it shows significant lateral variability seismically as illustrated in Figure 2 (bottom). To the west of the

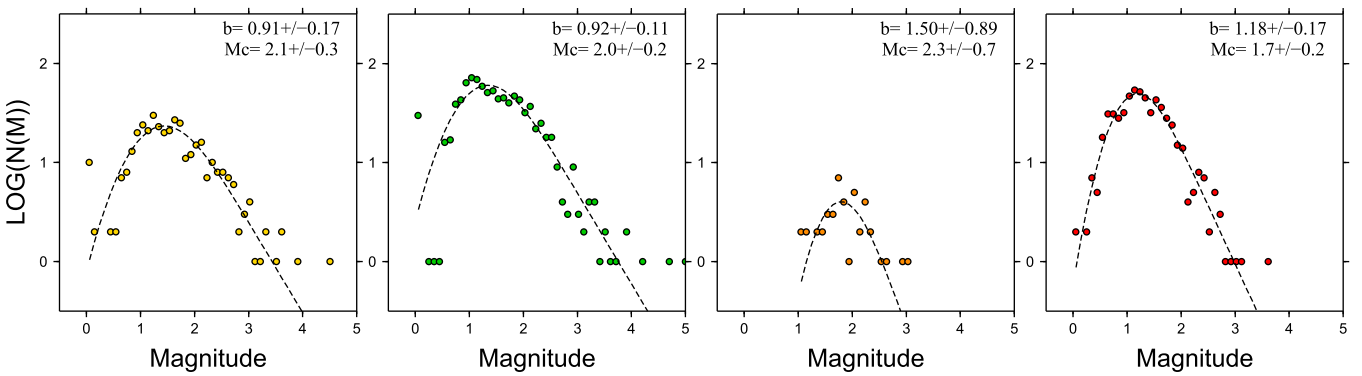

Figure 5. Earthquake magnitude distributions for each zone (colored circles—same colors as in Figure 2) using the catalog of this study. From left to right: Tekirdag basin, Central basin, Kumburgaz basin, and Cinarcik basin. Magnitude completeness (M_c) and *b*-values are obtained using the objective Bayesian method of *Ogata and Katsura* [1993] corresponding to the dotted black line.

MMF, on the Ganos segment the locking depth extends to 14 km [*Ergintav et al.*, 2007]. On the eastern part of the MMF, in the Cinarcik basin, it is estimated to be of the order of 10 km [*Ergintav et al.*, 2014]. At the center, in the Kumburgaz basin, the locking depth has been proposed to be very shallow (i.e., fully creeping domain) using a GPS profile which integrates stations over a broad domain (∼80 km along the fault) covering both the Kumburgaz and the Central basins (KB and CeB) [*Ergintav et al.*, 2014]. We will assume here that the later concerns mostly the Central basin (CeB) as shown in Figure 2 (bottom).

We use the Cinarcik basin as a reference in terms of fault behavior since the seismicity distribution in depth, $d_s \sim 11$ km, (Figure 4 for CB in red) corresponds to the locking depth of 10 km obtained by combining geodetic and seismicity data [*Ergintav et al.*, 2014]. We show that this is significantly different from the Central basin where most of the seismicity exists below the inferred GPS locking depth. It defines in the Central basin an extended brittle-ductile transition zone up to 14 km wide (from 3 to 17 km depth) where deep creeping might exist, as introduced by *Wdowinski* [2009] for the central segment of the San Jacinto Fault in California.

Figure 4 shows also the evolution of the cumulative number of events for each segment (in blue). Having a similar completeness magnitude in each segment (see Figure 5) allows to compare activity histories. A nearly constant background activity is taking place in the Tekirdag basin (TB) even if a moderate earthquake ($M = 4.5$) happens in this domain (gray circle in the figure). The same background rate emerges in the Central basin (CeB) between the three seismic crises related to $M > 4$ earthquakes where the cumulative number of events show significant steps. Surprisingly, these moderate events have a much larger influence with their aftershock sequences on the cumulative number of events than the $M = 4.5$ event in the Tekirdag basin (TB). The Kumburgaz basin (KB) also shows a constant background rate but significantly smaller. In the Cinarcik basin (CB), the background rate is also regular and higher with no specific aftershock sequences. Some swarms are noticeable and the lower rate for the year 2012 is mainly attributed to a change of the earthquake detection level in this area.

3.4. Lateral Variations of Magnitude Distribution

The *b*-values of each domain (TB, CeB, KB, CB) are computed from magnitude frequency distributions using the maximum-likelihood method of *Ogata and Katsura* [1993] (see Figure 5). The *b*-value of the central part (KB) is not well resolved because of the low level of seismicity. However, the distribution shows that the magnitude completeness of this segment is on the order of $M_c \sim 2$ meaning that the overall lack of seismicity along this segment is well resolved. Two important observations have to be made for the whole MMF. First the *b*-value of the western Marmara domain (TB and CeB) is significantly lower than that of the east Marmara domain (CB), $b \approx 0.90$ and $b \approx 1.20$, respectively. Figure 5 also confirms the larger number of $M > 3$ events in TB and CeB as suggested from Figures 2 and 3. Second, the *b*-values of the TB and CeB are very similar despite different aftershock behaviors after similar moderate events ($M \geq 4$): very little aftershock sequence in TB, major aftershock sequence in CeB as shown by the cumulative number of events.

The link between *b*-values and fault rheology (locked or creeping) has been previously addressed [e.g., *Wyss et al.*, 2004; *Scholz*, 2015]. It is observed for instance along the San Andreas Fault that locked segments exhibit a small *b*-value compared to creep segments with a large *b*-value. This is explained

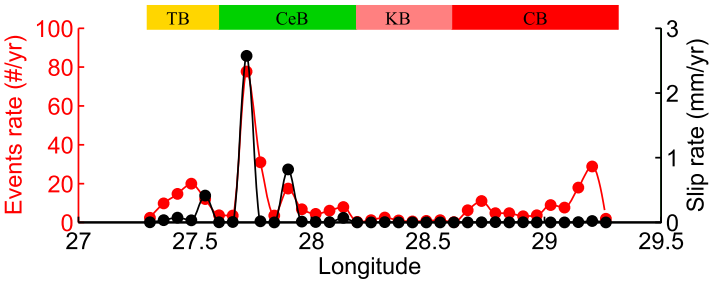

Figure 6. Profile along the MMF of the annual event rate (in red), per slices of 5 km along the fault. The color bar shows the extension of the four domains as defined in Figure 2. The black line shows the average seismic slip rate estimated from the method proposed by *Wdowinski* [2009] using a shear modulus $\mu = 35$ GPa and a fault thickness of 17 km.

from the following argument: high differential stresses in locked segment favor large earthquakes. Recent experimental results on Westerly granite samples have been proposed by *Goebel et al.* [2013] to support this link between the variability of the *b*-value and the differential loading stress. However, it has been shown by *Amitrano et al.* [2005] that this effect could also be explained by the change of a cut-off scale in the event size distribution when reaching failure and not necessarily by a change of *b*-value. Here we interpret the *b*-value fluctuations differently using the results of a quantitative mechanical model of distributed heterogeneous damage and its validation with a set of related laboratory experiments [*Amitrano*, 2003]. Indeed Amitrano shows that *b*-value changes are linked to the differences in the rheology of the material possibly related to the confining stress. Small *b*-values are shown to be related to a low internal friction angle and a ductile behavior obtained at high confining stress. High *b*-values are related to a high internal friction angle and a brittle behavior at low confining stress. These extended results suggest that regions with ductile behavior should have a low *b*-value and locked regions, a high *b*-value, contrary to the previous view. We checked that this relationship is valid on the San Jacinto Fault comparing the *b*-value of the deep creeping central segment to that of the locked southern segment. We then interpret the west Marmara segment as hosting a ductile dominated mode of rupture with high minimum stress while the PI segment on the eastern part rather behaves in a more brittle regime with low minimum stress. This partition is also compatible with a shallow locking depth in the west (TB and CeB) and a deeper locking depth to the east (CB).

3.5. Seismic Slip Rate

A rough estimate of the variation of the seismic coupling along the MMF can be estimated from the seismic slip rate. The seismic slip rate over a fault zone can be assessed from the seismic moment rate deduced from the seismicity catalog providing position, and magnitude of each event. *Wdowinski* [2009] used this approach for the San Jacinto Fault (SJF) which is part of the San Andreas Fault system. He compared the seismic slip rate estimated from the seismic catalog at depth to the geodetic slip rate measured from surface surveys. The seismic slip rate is estimated as: $v = \frac{1}{\mu A \Delta T} \sum_{\Delta T} M_0$ where μ is the shear modulus, A is the fault area, and ΔT is the duration of the catalog. The seismic moment M_0 for each event is deduced from the magnitude M using Kanamori's law [*Kanamori and Anderson*, 1975]: $\log(M_0) = 1.5M + 9.1$ although it is mostly valid for moderate to large earthquakes worldwide. He showed that the seismic slip rate along the SJF segment was locally high but still a small part of the geodetic slip rate: 0.5 mm/yr versus 12–22 mm/yr. He concluded that along this segment, elastic strain energy is released continuously both seismically and aseismically at the lower level of the seismogenic crust, at depths of 10–17 km, i.e., below the locking depth.

We applied the same approach to our catalog using $\mu = 35$ GPa from an average density of 2800 kg/m^3, a *P* wave velocity of $v_p = 6.2$ km/s, $v_p/v_s = 1.74$ where v_s is the *S* wave velocity [*Karabulut et al.*, 2011] and $\Delta T = 6$ year for the 2007–2012 period. Figure 6 shows the deduced slip rate for each domain using a seismogenic zone of 17 km. The profile of the event rate per year computed every 5 km along the MMF is also plotted.

From this calculation, we can hardly have a quantitative measure of the seismic coupling [*Scholz*, 2002] in each domain since the observation period is rather short (6 years) compared to the typical duration of the seismic cycle (~250 years). Nevertheless, a major observation emerges, the magnitude of the seismic slip rate is maximum in the Central basin (CeB). It is more than two orders of magnitude larger than in the Kumburgaz basin. In the Cinarcik basin (CB), the event rate is noticeably high in particular at the location of the segment termination clusters (i.e., the Tuzla cluster and the kink cluster). Interestingly, in the Tekirag basin (TB), the slip rate is significantly smaller than that of the Central basin (CeB) even if a $M = 4.5$ event happens.

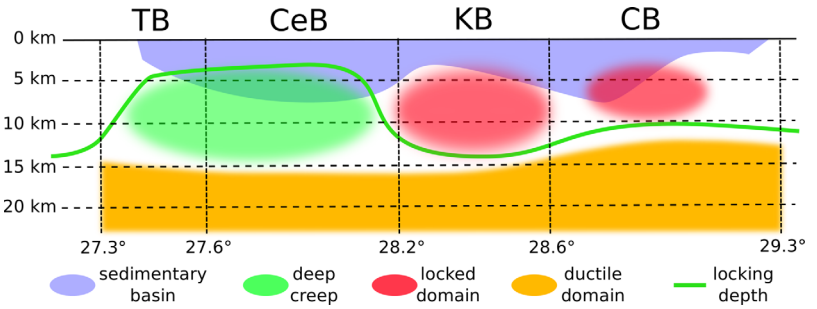

Figure 7. Interpretation of the MMF behavior (see text). The sedimentary basin depth is reproduced after *Bayrakci et al.* [2013].

Following the arguments of *Wdowinski* [2009], it suggests that the Central basin segment can be compared to the central part of the San Jacinto fault where a deep creep is proposed: similar high seismic slip rates (0.35 mm/yr versus 0.5 mm/yr), similar geodetic slip rates (23 mm/yr versus 17 mm/yr), similar strike slip tectonic configuration with a transition to a fully locked region (the Kumburgaz segment versus the Southern San Jacinto segment).

4. Conclusions

Our detailed study of the recent seismicity along the Main Marmara Fault provides new constraints on the degree of coupling on segments of the fault system in the Sea of Marmara. The major result is that the Central basin (CeB) segment behaves very differently from the rest of the MMF. The seismogenic depth $d_s \sim 13$ km defined from the 90% of the cumulative depth distribution, is much deeper than the geodetic locking depth $d_g \sim 0-3$ km [*Meade et al.*, 2002; *Ergintav et al.*, 2014]. In other words, most of the seismicity is taking place below the locking depth and above the ductile root of the fault. This is very different from the Cinarcik basin (CB) where $d_s \approx d_g$. The *b*-value of the Gutenberg-Richter distribution in CeB is significantly lower than the *b*-value of CB to the east (respectively, 0.9 and 1.2). This *b*-value contrast can be related to Amistrano's results [*Amitrano*, 2003] suggesting that the fault rheology is rather ductile to the west and brittle in the eastern MMF. Moreover, the seismic slip rate estimated from the cumulative seismic moment is more than two orders of magnitude larger in CeB than in the Kumburgaz segment (KB). As proposed by *Wdowinski* [2009], a high seismic slip rate in a domain below the locking depth is the signature of creep on the fault. Following all these arguments, the Central basin has all the indirect evidences of a domain where aseismic slip is significant. If so, it continuously relaxes significant shear stress without major seismic events ($M > 5$). Figure 7 summarizes our interpretation of the present behavior of the different basins of the MMF.

Our observations show also that the low level of seismicity on the Kumburgaz segment at the center of the MMF is being well resolved (comparison above the completeness magnitude). The seismicity rate there is far below the rate of west Marmara (CeB and TB). This segment exhibits a fully locked behavior similar to the Ganos segment which hosted the 1912 earthquake. In the Cinarcik basin, the situation looks intermediate as proposed by *Bohnhoff et al.* [2013] with seismicity mostly at the geodetic locking depth of ~10 km.

The Main Marmara Fault is a major seismic gap. In this context, the estimate of the locked segment area provides an estimate of the magnitude of the main forthcoming event assuming that the rupture will not enter significantly within creeping domains. With a length of 45 km and a seismogenic zone of 12 km for the locked zone, a shear modulus of 35 GPa, a tectonic velocity of 23 mm/yr and a seismic cycle of 250 year, the expected seismic moment of an event extending over the Kumburgaz segment is of the order of $1.1 \cdot 10^{20}$ Nm (i.e., $M_w \sim 7.3$). The two adjacent domains (the Central basin segment and the Princes Island segment) could be at the seat of moderate earthquakes or could rupture with the Kumburgaz segment. Moreover, the simple geometry and the very poor activity along the Kumburgaz segment are the signature of very little stress heterogeneities along the fault plane, making it a good candidate for supershear rupture [*Bouchon and Karabulut*, 2008]. If repeating foreshocks were expected to develop [*Bouchon et al.*, 2011], they should emerge at depth below or at the boundaries of the segment, possibly along the vertically extended deep observed swarms.

Appendix A: Comparison With KOERI Catalog

To test the quality of our catalog, we compare it with the catalog of KOERI for the same period and same region (3094 events, out of which 873 are along the MMF) (http://www.koeri.boun.edu.tr/sismo). The KOERI catalog is compiled from permanent stations only. First, we show the map and depth section of the seismicity obtained from this catalog (see Figure A1).

Second, we compare the Gutenberg-Richter distribution along the MMF domain using the same technique as in Figure 5 (see Figure A2) but using three subcatalogs: events only extracted from the KOERI catalog, events that exist in the KOERI catalog but using our local magnitude estimate and events entirely from our catalog.

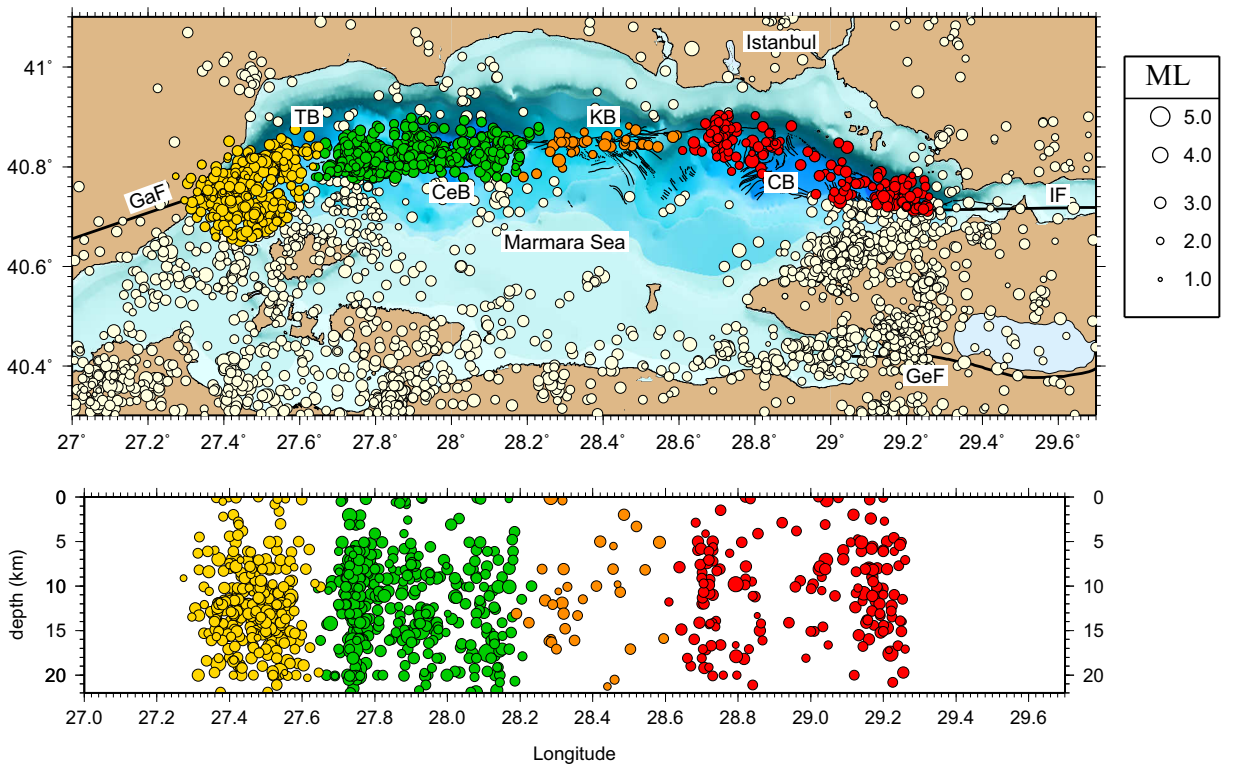

Figure A1. (top) Map and (bottom) depth section of the seismicity along the MMF in the Marmara Sea during the period 2007–2012 from the KOERI catalog using only permanent stations.

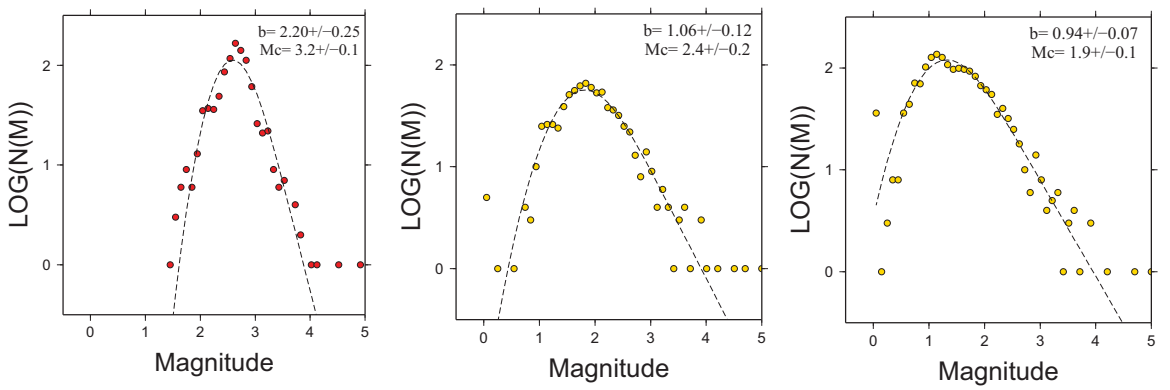

Figure A2. Comparison of the earthquake magnitude distribution for the MMF zone defined as the merge of TB, CeB, KB, and CB domains, using (left) events from the KOERI catalog; (middle) events from the present catalog that exist in the KOERI catalog; and (right) all events from the present catalog.

Acknowledgments
V. Durand, G. Daniel, M.P. Bouin, M. Aktar, A. Kömeç-Multu, L. Geli, P. Henry, S. Ergintav, R. Reilinger, O. Konca, M. Bohnhoff, and A.D. Ozbakir are deeply acknowledged for very fruitful discussions and data providing. We thank R. Reilinger and an anonymous reviewer for constructive reviews that helped to improve this paper. A. Steyer provided useful technical support. KOERI and TUBITAK-MRC are deeply acknowledged for providing the seismic data. The project was supported by FP-7 REAKT and MARSITE projects, Electricité de Strasbourg donation, ANR MODALSIS and SUPNAF grants and USIAS SEISNAF grant.

References

Amitrano, D. (2003), Brittle-ductile transition and associated seismicity: Experimental and numerical studies and relationship with the b value, *J. Geophys. Res.*, *108*(B1), 2044, doi:10.1029/2001JB000680.
Amitrano, D., J. R. Grasso, and G. Senfaute (2005), Seismic precursory patterns before a cliff collapse and critical point phenomena, *Geophys. Res. Lett.*, *32*, L08314, doi:10.1029/2004GL022270.
Armijo, R., et al. (2005), Submarine fault scarps in the Sea of Marmara pull-apart (North Anatolian Fault): Implications for seismic hazard in Istanbul, *Geochem. Geophys. Geosyst.*, *6*, Q06009, doi:10.1029/2004GC000896.
Bayrakci, G., et al. (2013), 3-D sediment-basement tomography of the Northern Marmara trough by a dense OBS network at the nodes of a grid of controlled source profiles along the North Anatolian Fault, *Geophys. J. Int.*, *194*(3), 1335–1357.
Bohnhoff, M., F. Bulut, G. Dresen, P. E. Malin, T. Eken, and M. Aktar (2013), An earthquake gap south of Istanbul, *Nat. Commun.*, *4*.
Bouchon, M., and H. Karabulut (2008), The aftershock signature of supershear earthquakes, *Science*, *320*(5881), 1323–1325.
Bouchon, M., H. Karabulut, M. Aktar, S. Ozalaybey, J. Schmittbuhl, and M. Bouin (2011), Extended nucleation of the 1999 m-w 7.6 Izmit earthquake, *Science*, *331*, 877–880.
Bulut, F., M. Bohnhoff, W. L. Ellsworth, M. Aktar, and G. Dresen (2009), Microseismicity at the North Anatolian Fault in the Sea of Marmara offshore Istanbul, NW Turkey, *J. Geophys. Res.*, *114*, B09302, doi:10.1029/2008JB006244.
Çakir, Z., S. Ergintav, H. Özener, U. Dogan, A. M. Akoglu, M. Meghraoui, and R. Reilinger (2012), Onset of aseismic creep on major strike-slip faults, *Geology*, *40*(12), 1115–1118.
Earle, P. S., and P. M. Shearer (1994), Characterization of global seismograms using an automatic-picking algorithm, *Bull. Seismol. Soc. Am.*, *84*(2), 366–376.
Emre, O., T. Duman, S. Özalp, H. Elmac i, Ş. Olgun, and F. Şaroğlu (2013), 1/1.125.000 Ölçekli türkiye diri fay haritas i, Technical Report, Maden Tetkik ve Arama Genel Müdürlüğü, Ankara, Türkiye.
Ergintav, S., U. Doğan, C. Gerstenecker, R. Cakmak, A. Belgen, H. Demirel, C. Ayd in, and R. Reilinger (2007), A snapshot (2003–2005) of the 3D postseismic deformation for the 1999, Mw = 7.4 Izmit earthquake in the Marmara region, Turkey, by first results of joint gravity and GPS monitoring, *J. Geodyn.*, *44*(1), 1–18.
Ergintav, S., R. Reilinger, R. Çakmak, M. Floyd, Z. Çakr, U. Doğan, R. King, S. McClusky, and H. Özener (2014), Istanbul's earthquake hot spots: Geodetic constraints on strain accumulation along faults in the Marmara seismic gap, *Geophys. Res. Lett.*, *41*, 5783–5788, doi:10.1002/2014GL060985.
Fialko, Y. (2006), Interseismic strain accumulation and the earthquake potential on the southern San Andreas Fault system, *Nature*, *441*(7096), 968–971.
Geli, L., et al. (2008), Gas emissions and active tectonics within the submerged section of the North Anatolian Fault zone in the Sea of Marmara, *Earth Planet. Sci. Lett.*, *274*(1–2), 34–39.
Goebel, T., D. Schorlemmer, T. Becker, G. Dresen, and C. Sammis (2013), Acoustic emissions document stress changes over many seismic cycles in stick-slip experiments, *Geophys. Res. Lett.*, *40*, 2049–2054, doi:10.1002/grl.50507.
Havskov, J., and L. Ottemoller (1999), Seisan earthquake analysis software, *Seismol. Res. Lett.*, *70*(5), 532–534.
Hergert, T., and O. Heidbach (2010), Slip-rate variability and distributed deformation in the Marmara Sea fault system, *Nat. Geosci.*, *3*, 132–135, doi:10.1038/NGEO739.
Imren, C., X. Le Pichon, C. Rangin, E. Demirbağ, B. Ecevitoğlu, and N. Görür (2001), The North Anatolian Fault within the Sea of Marmara: A new interpretation based on multi-channel seismic and multi-beam bathymetry data, *Earth Planet. Sci. Lett.*, *186*(2), 143–158.
Kanamori, H., and D. L. Anderson (1975), Theoretical basis of some empirical relations in seismology, *Bull. Seismol. Soc. Am.*, *65*(5), 1073–1095.
Karabacak, V., E. Altunel, and Z. Cakir (2011), Monitoring aseismic surface creep along the North Anatolian Fault (Turkey) using ground-based LIDAR, *Earth Planet. Sci. Lett.*, *304*(1), 64–70.
Karabulut, H., J. Schmittbuhl, S. Özalaybey, O. Lengliné, A. Kömeç-Multu, V. Durand, M. Bouchon, G. Daniel, and M. Bouin (2011), Evolution of the seismicity in the eastern Marmara Sea a decade before and after the 17 August 1999 Izmit earthquake, *Tectonophysics*, *510*(1–2), 17–27, doi:10.1016/j.tecto.2011.09.009.
Kissling, E., W. Ellsworth, D. Eberhart-Phillips, and U. Kradolfer (1994), Initial reference models in local earthquake tomography, *J. Geophys. Res.*, *99*, 19,635–19,646.
Lengliné, O., and D. Marsan (2009), Inferring the coseismic and postseismic stress changes caused by the 2004 mw = 6 Parkfield earthquake from variations of recurrence times of microearthquakes, *J. Geophys. Res.*, *114*, B10303, doi:10.1029/2008JB006118.
Lengliné, O., J. Elkhoury, G. Daniel, J. Schmittbuhl, R. Toussaint, J.-P. Ampuero, and M. Bouchon (2012), Interplay of seismic and aseismic deformations during earthquake swarms: An experimental approach, *Earth Planet. Sci. Lett.*, *331*, 215–223.
Le Pichon, X., et al. (2001), The active Main Marmara Fault, *Earth Planet. Sci. Lett.*, *192*, 595–616.
Le Pichon, X., C. Imren, C. Rangin, A. M. C. Şengör, and M. Siyako (2014), The South Marmara Fault, *Int. J. Earth Sci.*, *103*, 219–231.
Lienert, B. R., and J. Havskov (1995), A computer program for locating earthquakes both locally and globally, *Seismol. Res. Lett.*, *66*(5), 26–36.
McClusky, S., et al. (2000), Global positioning system constraints on plate kinematics and dynamics in the eastern Mediterranean and Caucasus, *J. Geophys. Res.*, *105*, 5695–5719.
Meade, B. J., B. H. Hager, S. C. McClusky, R. E. Reilinger, S. Ergintav, O. Lenk, A. Barka, and H. Özener (2002), Estimates of seismic potential in the Marmara Sea region from block models of secular deformation constrained by Global Positioning System measurements, *Bull. Seismol. Soc. Am.*, *92*(1), 208–215.
Ogata, Y., and K. Katsura (1993), Analysis of temporal and spatial heterogeneity of magnitude frequency distribution inferred from earthquake catalogues, *Geophys. J. Int.*, *113*(3), 727–738.
Reverso, T., D. Marsan, and A. Helmstetter (2015), Detection and characterization of transient forcing episodes affecting earthquake activity in the Aleutian Arc system, *Earth Planet. Sci. Lett.*, *412*, 25–34.
Rubin, A. M., D. Gillard, and J.-L. Got (1999), Streaks of microearthquakes along creeping faults, *Nature*, *400*(6745), 635–641.
Savage, J., and R. Burford (1973), Geodetic determination of relative plate motion in central California, *J. Geophys. Res.*, *78*, 832–845.
Scholz, C. H. (2002), *The Mechanics of Earthquakes and Faulting*, Cambridge Univ. Press, Cambridge, U. K.
Scholz, C. H. (2015), On the stress dependence of the earthquake *b* value, *Geophys. Res. Lett.*, *42*, 1399–1402, doi:10.1002/2014GL062863.
Segall, P. (2010), *Earthquake and Volcano Deformation*, Princeton Univ. Press, Princeton, N. J.
Shelly, D. R. (2010), Migrating tremors illuminate complex deformation beneath the seismogenic San Andreas Fault, *Nature*, *463*(7281), 648–652.

Waldhauser, F., and W. L. Ellsworth (2000), A double-difference earthquake location algorithm: Method and application to the northern Hayward fault, California, *Bull. Seismol. Soc. Am.*, *90*(6), 1353–1368.

Waldhauser, F., W. L. Ellsworth, D. P. Schaff, and A. Cole (2004), Streaks, multiplets, and holes: High-resolution spatio-temporal behavior of Parkfield seismicity, *Geophys. Res. Lett.*, *31*, L18608, doi:10.1029/2004GL020649.

Wdowinski, S. (2009), Deep creep as a cause for the excess seismicity along the San Jacinto fault, *Nat. Geosci.*, *2*(12), 882–885.

Weaver, C. S., and D. P. Hill (1978), Earthquake swarms and local crustal spreading along major strike-slip faults in California, *Pure Appl. Geophys.*, *117*(1–2), 51–64.

Wyss, M., C. G. Sammis, R. M. Nadeau, and S. Wiemer (2004), Fractal dimension and b-value on creeping and locked patches of the San Andreas Fault near Parkfield, California, *Bull. Seismol. Soc. Am.*, *94*(2), 410–421.